3

Determination of Binding Kinetics between Proteins with Multiple Nonidentical Binding Sites by SPR Flow Cell Biosensor Technology

Kristmundur Sigmundsson[1,4], Nicole Beauchemin[3], Johan Lengqvist[2,5] and Björn Öbrink[1]

[1]*Department of Cell and Molecular Biology, Karolinska Institutet, Stockholm,*
[2]*Department of Medical Biophysics and Biochemistry, Karolinska Institutet, Stockholm,*
[3]*Goodman Cancer Research Centre, McGill University, Montreal, QC,*
[4]*Present address: Department of Medical Biophysics and Biochemistry, Karolinska Institutet, Stockholm,*
[5]*Present address: Department of Molecular Toxicology, Safety Assessment, AstraZeneca Research and Development, Södertälje,*
[1,2,4,5]*Sweden*
[3]*Canada*

1. Introduction

Protein-protein binding interactions are crucial in signaling networks that regulate cellular functions in health and disease. A large number of membrane and cytoplasmic proteins participate in those networks, and a complete understanding of their functional activities at the cellular level would require comprehensive analysis of the kinetics of the various protein interactions. This is, however, a herculean task due to both the multitude of interacting proteins and the complexity of the individual pairwise binding interactions. The latter are in many cases not simple 1:1 binding reactions but a result of simultaneous interactions between several distinct binding sites. In an initial attempt to tackle this challenge we have developed new algorithms and experimental procedures to determine the binding kinetics of the cell adhesion receptor CEACAM1-L and the protein tyrosine phosphatase SHP-1 (Fig. 1). CEACAM1-L is a signal-regulating cell surface-associated transmembrane protein that regulates a plethora of basic biological events including cell proliferation and motility, apoptosis, tissue morphogenesis, immune reactions and microbial infections, vasculogenesis and angiogenesis, and cancer growth and invasion (Gray-Owen & Blumberg, 2006; Müller et al., 2009; Singer et al., 2010). Many of CEACAM1-L's regulatory activities are a result of its binding and activation of Src-family kinases and the protein tyrosine phosphatases SHP-1 and SHP-2. The cytoplasmic domain of CEACAM1-L contains two phosphotyrosine-based ITIM sequences, pY488 and pY515, that bind to SH2 domains in the kinases and phosphatases (Fig. 1). The kinases have one SH2 domain whereas the phosphatases have two SH2 domains, N-SH2 and C-SH2, arranged in tandem. Thus, there is a potential for at least four different binding interactions between CEACAM1-L and SHP-1 or SHP-2. Here we have focussed on the binding interactions between the cytoplasmic domain of

CEACAM1-L and the SH2 domains of SHP-1, which were studied in an SPR-based flow cell biosensor.

To be able to analyze such a complex system, with several distinct binding sites in both of the interacting molecules, we started by characterizing the interactions between the single binding sites, using peptides and protein domains. The resulting parameters were then used as building blocks for more elaborate analyses of the interactions of the tandem N,C-$(SH2)_2$ domain with the double-tyrosine-phosphorylated cytoplasmic domain of CEACAM1-L. The major questions that we addressed with this approach were: which complexes are formed between the CEACAM1-L cytoplasmic domain and the tandem SH2-domain of SHP-1, what kind of kinetics do they obey, and which of them are of physiological relevance. To that end we had to develop new reaction schemes based on plausible interactions, and translate them into equations and algorithms that could be used for curve fitting analysis of recorded sensorgrams. The analyses demonstrated that both the N-SH2 and C-SH2 domains of SHP-1 participated in binding to the two ITIM sequences in CEACAM1-L. Interestingly, our approach led to the discovery of a second phosphotyrosine binding site in the C-SH2 domain, which differed kinetically from the other C-SH2 binding site. At physiological temperature, the most pronounced complex that was formed was a double-docked form, in which the CEACAM1-L pY488 motif occupied the N-SH2 binding site and the pY515 motif occupied one of the two phosphotyrosine binding sites in the C-SH2 domain.

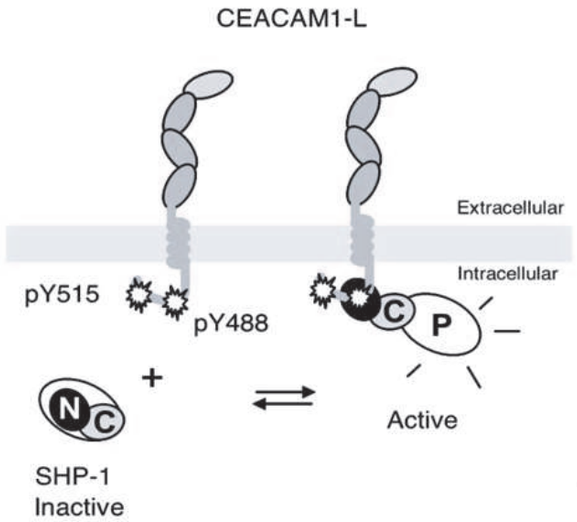

Fig. 1. Cartoon of CEACAM1-L, SHP-1 and a hypothetical interaction complex. Murine CEACAM1-L has an intracellular domain of 73 amino acids including two phosphorylatable tyrosine residues, Y488 and Y515. SHP-1 has two SH2 domains (labelled N and C) and a C-terminal phosphatase domain (P). The phosphatase is autoinhibited when undocked. SH2-domain interactions with phosphotyrosine-containing sequence motifs initiate a conformational change leading to phosphatase activation.

2. Experimental procedures

2.1 Peptides

Peptides spanning the Y488 and Y515 regions of mouse CEACAM1-L were purchased from K. J. Ross-Petersen AS (Horsholm, Denmark). These included both unphosphorylated and

tyrosine-phosphorylated forms of N-terminally biotinylated dodecameric peptides: VDDVAY(488)TVLNFN, ATETVY(515)SEVKKK, and N-terminally cysteinylated eicosameric and pentadecameric peptides: CKVDDVAY(488)TVLNFNSQQPNR and CPRATETVY(515)SEVKKK, respectively. Additionally, a scrambled derivative of the unphosphorylated Y488 dodecapeptide, Biotin-LANDFVNDTVYV, was purchased from the same producer. All peptides were highly homogeneous and > 95 % pure as demonstrated by amino acid analysis, HPLC, and MALDITOF mass spectrometry.

2.2 Recombinant proteins

The construction of recombinant proteins of single SH2 domains and the tandem form N,C-$(SH2)_2$ of mouse SHP-1, and of the cytoplasmic part of mouse CEACAM1-L fused with GST using the pGEX-2T vector system, has been described previously (Beauchemin et al. 1997). Proteins were produced in *Escherichia coli* BL21. Protein synthesis was induced with IPTG (0.2 mM). The tyrosine phosphorylated cytoplasmic part of CEACAM1-L (GST-Lcyt-[pY488/pY515]) was produced in *Epicurian coli* TKX1 (#200124, Stratagene), inducing protein synthesis simultaneously with IPTG (0.2 mM) and IAA (0.1 mM). Purification of the GST fusion proteins was performed by affinity adsorption on glutathione-Sepharose according to a standard protocol from the manufacturer (Amersham). Buffer exchange and further purification of recombinant proteins was carried out on a Superose 12 prepacked column attached to a FPLC 500 system (Pharmacia AB), equilibrated in 10 mM Hepes, 150 mM NaCl, 3.4 mM EDTA, and 0.005% surfactant P20, pH 7.4 (HBS). Protein purity was confirmed by SDS-PAGE. Concentrations of purified GST-N-SH2, GST-C-SH2, GST-N,C-$(SH)_2$ and GST-Lcyt proteins were determined by absorption spectroscopy, using the following molar absorptivity values (ε in $M^{-1}cm^{-1}$, at 280 nm): 51730, 57480, 69630 and 43480, respectively. In the protein interaction measurements, the active concentrations of the analyte proteins were double-checked by the BIAcore-based procedure described in (Sigmundsson et al., 2002). For GST removal, recombinant proteins were treated with 100 units of thrombin per 3 mg fusion protein per 1 ml at 4 ˚C, for 48 h, with mild swirling. The calculated molecular masses of non-cleaved fusion proteins were: GST-N-SH2 = 37.5 kDa, GST-C-SH2 = 39.0 kDa and GST-N,C-$(SH)_2$ = 51.1 kDa. The calculated molecular masses of thrombin cleaved products were: N-SH2 = 11.3 kDa, C-SH2 = 12.9 kDa, N,C-$(SH)_2$ = 24.9 kDa and GST = 26.2 kDa. The tyrosine phosphorylation of GST-Lcyt was determined by nanoelectrospray ionization mass spectrometry using a QTQF1 instrument (Waters), analysing both intact full size protein and trypsinized fragments.

2.3 Protein interaction measurements

Interaction measurements based on surface plasmon resonance (SPR) detection were carried out with a BIAcore 2000 instrument (BIAcore AB, Uppsala, Sweden).

2.4 Ligand immobilization

Peptides were immobilized on CM5 Sensor Chips, either by binding via the N-terminal biotin groups to immobilized streptavidin (SA), or via direct coupling by thiol-disulphide exchange. Carboxymethyl-modified dextran surfaces were activated according to a standard procedure, with an injection of 0.05 M NHS/0.2 M EDC for 7 min. High density streptavidin chips (SA ≈ 2000 RU) were prepared by injection of 140 µl of freshly prepared SA (50 µg/ml in 5 mM acetate buffer, pH 4.5) at 10 µl/min. This resulted in 1995 – 2025 RU of immobilized streptavidin per lane after blocking of remaining reactive esters with two injections of 1 M

ethanolamine-HCl, pH 8.5 for 2 min each. Low density streptavidin chips (SA ≈ 1000 RU) were prepared by injection of 40 µl of SA (50 µg/ml) and blocking as described above, which resulted in 980 – 1100 RU of SA per lane. N-terminally biotinylated dodecameric peptides were dissolved in DMSO to give stock solutions of 3.5 g/l. Prior to immobilization, the stocks were diluted to 50 µg/ml in HBS and then injected into separate lanes at 20 µl/min for one minute. Finally, the lanes were washed separately by four injections of 6 M guanidine-HCl/HBS, pH 7.4 for 1 min each and injections of 4 M LiCl/HBS for 1 min and 0.25 % P20/HBS for 1 min, respectively. The levels of stably immobilized peptides were 200 – 240 RU and 65-80 RU per lane, for high and low density SA surfaces, respectively.

For preparation of low density peptide surfaces, N-terminally cysteinylated peptides were immobilized via direct coupling by thiol-disulphide exchange. For this purpose, NHS/EDC activated surfaces were modified by interaction with a freshly prepared solution of 80 mM PDEA (thiol coupling reagent) in 0.1 M borate buffer pH 8.5 for 4 min, by injection of 40 µl at 10 µl/min, followed by a 4 min blocking step with 1 M ethanolamine-HCl, pH 8.5, prior to peptide injections. Peptides were dissolved in DMSO at 2 mM concentration and were diluted with 5 mM acetate buffers to the indicated concentrations immediately before immobilization as follows: CKVDDVAY(488)TVLNFNSQQPNR 0.4 µM at pH 4.5, CKVDDVA-pY(488)-TVLNFNSQQPNR 10.0 µM at pH 3.9, CPRATETVY(515)SEVKKK 0.2 µM at pH 4.5, and CPRATETV-pY(515)-SEVKKK 0.5 µM at pH 4.5. Levels of stably immobilized peptides were 35 ± 5 RU per lane 1 and 2 for the pY515 and Y515 peptides respectively, and 16 ± 5 RU for the pY488 peptide on lane 3, as determined after blocking of remaining reactive surface 2-pyridinyldithio-groups with freshly prepared 6 mM L-cysteine in 5 mM acetate, pH 4.5 for 2 min, followed by washing with 0.25% P20/HBS. If assuming 100% binding capacity of these two surfaces the theoretical saturation level, i.e. R_{Max} with regard to N,C-$(SH)_2$ as the analyte, was c:a 120 RU and 510 RU, for the pY488 and pY515 surfaces, respectively. The non-phosphorylated Y515 peptide on lane 2 was applied as the reference surface. For preparation of peptide-free reference surfaces (lane 4), blocking was performed by injection of the L-cysteine solution for 15 min at 10 µl/min.

For immobilization of the GST-Lcyt-pY protein, anti-GST antibody was amine-coupled to CM5 Sensor Chips. For this purpose the carboxymethyl-modified dextran surfaces were activated according to standard procedures. The antibody was diluted in 10 mM Na-acetate buffer, pH 5.0, according to a standard protocol from the manufacturer and injected at 10 µl/min to a final immobilization level of 1000 ± 100 RU per lane. The surfaces were washed ten times with 20 µl of 20 mM glycine, pH 2.2, followed by two washes with 20 µl 2 M LiCl/HBS and one wash with 20 µl of 0.2 % P20/HBS, at a flow rate of 10 µl/min. GST-Lcyt-pY was immobilized on lane 2 at a concentration of 0.2 mg/ml in HBS at a flow rate of 10 µl/min, for 6 min. A saturation level of c:a 112 RU was reached, and verified by an additional injection of 20 µl of 0.5 mg/ml GST-Lcyt-pY, which did not add to the immobilized amount of ligand. Lane 1 was saturated with GST and used as the reference lane. When loading the reference lane, 0.4 mg/ml GST in HBS was flushed over both lane 1 and lane 2, for 10 min. This resulted in c:a 95 RU binding of GST to lane 1, while no change was obtained in lane 2. Surfaces were washed 10 times with 1.5 M LiCl/HBS with no detectable decrease in ligand levels.

2.5 Protein interaction analyses

Samples were kept at 2° C prior to injection. All interaction analyses were performed in HBS at a flow of 20 µl/min. In all SPR assays involving peptide ligands, phosphorylated

peptides were placed in flow cells 1 and 3. Flow cell 2 was loaded with unphosphorylated peptide or a scrambled unphosphorylated peptide and was used as a reference for unspecific binding and background subtraction. Flow cell 4 was kept free of ligand (peptide), but received the complete treatment of activation and inactivation. This flow cell was used as an independent control to monitor differences in refractive indices of sample and running buffer and to monitor background adsorption to the dextran (or dextran-SA) surface. A monoclonal anti-phosphotyrosine antibody (PY99) was used to confirm equal loadings of phosphotyrosine peptides in flow cells 1 and 3. For qualitative binding studies non-cleaved and cleaved recombinant proteins were flushed over N-terminally biotinylated dodecameric peptides at 25˚ C, immobilized on both high and low density SA chips. Low density surfaces with N-terminally cysteinylated peptides (15-30 RU) were used in SPR assays aimed to determine kinetic constants. For this purpose, recombinant proteins cleaved from GST were injected at different concentrations in a randomized order with a total of 3 injections per concentration. This process was repeated at 5˚, 15˚, 25˚, 35˚, and 37° C. Regeneration of ligand surfaces containing disulfide-linked peptides was performed with a 1 min pulse of 4 M LiCl/HBS, followed by a 1 min pulse of 0.25 % P20/HBS, at 20 µl/min. Interactions with the GST-Lcyt-pY ligand were performed in triplicates at 25˚ C. The GST-Lcyt-pY ligand surface was regenerated with a 1 min pulse of 1.5 M LiCl/HBS, followed by a 1 min pulse of 0.20 % P20/HBS. To optimize the interaction profiles used for kinetic calculations, the recorded primary responses were processed in a double background subtraction routine. For this purpose, triplicate injections of running buffer were recorded at all temperatures. Thereafter, the averaged buffer profile of each flow cell, at a given temperature, was subtracted from the primary response profiles of individual sample injections. Then, the reference lane response was subtracted from the ligand lane response.

2.6 Interaction models

The recorded profiles of N,C-$(SH2)_2$ interactions with immobilized CEACAM1 peptides (pY488 and pY515) were compared with three models, based on plausible interaction mechanisms. The interaction of N,C-$(SH2)_2$ with GST-Lcyt-[pY488/pY515] required a specific model, described below as Model 4. All the models assumed a mass transport limited process based on the two compartment model (Myszka et al., 1997).

2.6.1 Model 1: A simple bimolecular interaction

The primary model for a simple interaction of two components, where one is in solution (analyte: A) and the other is attached to a surface (ligand: L) is defined as a two step process

$$A_{\text{bulk}} \underset{k_c}{\overset{k_c}{\rightleftharpoons}} A_{\text{surface}} + L \underset{k_d}{\overset{k_a}{\rightleftharpoons}} AL$$

where the first step is the mass transport of the analyte between the bulk flow and the surface (characterized by the k_c coefficient). The second step describes the interactions at the surface, i.e. the rate of complex (AL) formation and dissociation.

2.6.2 Model 2: A bimolecular interaction of an analyte with two binding sites

The tandem shaped N,C-$(SH2)_2$ of SHP-1 represents a type of analyte, carrying at least two binding sites per molecule. These two sites can possibly compete in binding to the same phosphotyrosine motif (ligand: L). Model 1 cannot be applied to such an interaction, except in the rare case where both sites (domains) would have identical interaction kinetics. A model which takes into account the different kinetics of two binding sites on the same analyte, interacting with a uniform ligand, has the form

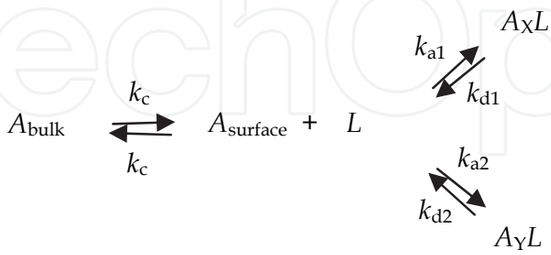

Referring to N,C-$(SH)_2$ as the analyte, the rate constant pairs k_{a1}, k_{d1} and k_{a2}, k_{d2} describe the kinetics of complexes formed via the N-SH2 and C-SH2 domains, respectively. This model assumes a stoichiometry of 1:1 and a low density of the surface bound ligand.

2.6.3 Model 3: A bimolecular interaction of an analyte with three binding sites

This is an extension of Model 2, accounting for a third binding site in the analyte molecule. The rate constant pair k_{a3} and k_{d3}, characterizes the kinetics of a complex ($A_Z L$) formed via this additional site, resulting in

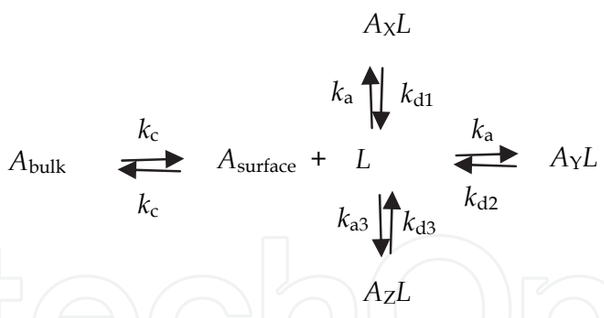

2.6.4 Model 4: A bimolecular interaction between a ligand with two binding sites and an analyte with three binding sites

A specific model was designed to address the interaction of the N,C-$(SH2)_2$ tandem domain with the entire CEACAM1-L cytoplasmic domain phosphorylated on both tyrosine residues. The model was restricted to AL binary complex forms, i.e. simultaneous binding of one A molecule to two L molecules, or of two A molecules to one L molecule, was excluded. All combinations of single docking between one of the three analyte sites and one of the two ligand sites were included. Furthermore, we included all permutations of second docking events allowing the formation of double docked AL forms from single docked forms. The reactions in this model are displayed in Figure 4C.

2.6.5 Mathematical description of models 1-4

A mathematical description of the interaction models is provided here in sets of coupled first order differential equations. These equations were used in curve fit routines for kinetics analyses, including the estimation of rate constants from experimentally obtained data. The analyte concentration in the bulk and at the surface is defined by $[A_B]$ and $[A_S]$, respectively, the concentration of free ligand binding sites as $[L]$, and a surface bound complex of analyte and ligand as $[AL]$, all in the unit of μM. Different binding sites in the analyte molecule are referred to as X, Y and Z. Association and dissociation rate constants are defined as k_a or k_{ax}, and k_d or k_{dx}, respectively, where x defines a particular reaction. Unless stated differently, k_a and k_d are in the units of $M^{-1}s^{-1}$ and s^{-1}, respectively. The mass transport between the bulk flow and the surface is defined by a coefficient k_c. h_d is a characteristic height of the diffusion layer that links the change in concentration expressed per surface area ($[AL]$) and per volume ($[A_S]$). Calculations of h_d and k_c were performed in the same manner as we have described previously (Sigmundsson et al., 2002).

Model 1:

$$d[A_S]/dt = (k_c([A_B] - [A_S]) - k_a[A_S][L] + k_d[AL])/h_d \tag{1.1}$$

$$d[AL]/dt = k_a[A_S][L] - k_d[AL] \tag{1.2}$$

Model 2:

$$d[A_S]/dt = (k_c([A_B] - [A_S]) - (k_{a1} + k_{a2})[A_S][L] + k_{d1}[A_X L] + k_{d2}[A_Y L])/h_d \tag{2.1}$$

$$d[A_X L]/dt = k_{a1}[A_S][L] - k_{d1}[A_X L] \tag{2.2}$$

$$d[A_Y L]/dt = k_{a2}[A_S][L] - k_{d2}[A_Y L] \tag{2.3}$$

$$d[AL_{Total}]/dt = (k_{a1} + k_{a2})[A_S][L] - k_{d1}[A_X L] - k_{d2}[A_Y L] \tag{2.4}$$

Model 3:

$$d[A_S]/dt = (k_c([A_B] - [A_S]) - (k_{a1} + k_{a2} + k_{a3})[A_S][L] + k_{d1}[A_X L] + k_{d2}[A_Y L] + k_{d3}[A_Z L])/h_d \tag{3.1}$$

$$d[A_X L]/dt = k_{a1}[A_S][L] - k_{d1}[A_X L] \tag{3.2}$$

$$d[A_Y L]/dt = k_{a2}[A_S][L] - k_{d2}[A_Y L] \tag{3.3}$$

$$d[A_Z L]/dt = k_{a3}[A_S][L] - k_{d3}[A_Z L] \tag{3.4}$$

$$d[AL_{Total}]/dt = (k_{a1} + k_{a2} + k_{a3})[A_S][L] - k_{d1}[A_X L] - k_{d2}[A_Y L] - k_{d3}[A_Z L] \tag{3.5}$$

Model 4:

The two ligand binding sites are referred to as α (pY488) and β (pY515). The three analyte binding sites are referred to as X, Y and Z (N-SH2, C2-SH2 and C1-SH2, respectively). The model takes into account three different ligand forms, which in our case refer to the tyrosine-phosphorylation status of the ligand. In this respect the ligand is divided into three populations: L^{α}, L^{β} and $L^{\alpha\beta}$, for mono- and di-phosphorylated forms. The fractions of these forms with regard to the total amount of phosphorylated ligand units are defined with $\mathbf{\Pi}$, $\mathbf{\Psi}$ and $\mathbf{\Omega}$, respectively. The detected response signal R, measured by an SPR-based sensor is proportional to the amount of complex formed at the detector surface multiplied by the factor MwG, i.e., $R = MwG[AL]$, where Mw is the molecular mass of the analyte and G is a factor converting the concentration to R values (G = 10000 R cm²/g of protein). When all the immobilized ligand has been fully bound into an AL complex, $R = R_{Max}$ (i.e., a theoretical maximum value). The contribution of the different [AL] complexes to the response signal (R) can now be referred to as follows: $R^{\alpha X} = [A^X L^{\alpha}]$, defines the amount of a complex docked via the α-site in the ligand and the X-site in the analyte. The total response of complexes docked via the α site is defined as R^{α}. The amount of a double docked complex with a [α-X/β-Z] configuration, is defined as $R^{\alpha X \beta Z}$. The total response of all double docked forms is defined as $R^{\alpha\beta}$. Complexes of di-phosphorylated single-docked ligands are defined with the subscription 2P, eg. $R^{\alpha X}{}_{2P}$. Association constants labeled with stars (k_a^* and k_a^{**}) define the second association steps giving rise to double docked forms. These constants have the unit of s^{-1}. To keep the amount of fit parameters at minimum it is assumed that a binding between two interacting sites, whether formed via a primary or a secondary docking event, dissociates with the same probability. Thus, the interactions described by k_{a1}, k_{a1}^*, k_{a1}^{**}, all share the same dissociation constant, k_{d1}. The full size model includes 32 parameters. Thereof 24 are rate constants. The model is easily adjusted for fewer reactions. The version used to calculate the data presented in Figure 4 included 20 parameters, of which 16 were rate constants. After the identification and elimination of non-existing reactions, and after the identification of parameters which could be fixed, the fit variables could be limited to 5, 4 of which representing unknown rate constants, and R_{Max} being the fifth global variable.

$$\frac{d[A_S]}{dt} = (k_c([A_B] - [A_S]) - (k_{a1} + k_{a2} + k_{a3})[A_S]\frac{(\Pi R_{Max} - R^{\alpha})}{M_w G}$$
$$+\frac{(k_{d1}R^{\alpha X} + k_{d2}R^{\alpha Y} + k_{d3}R^{\alpha Z})}{M_w G} - (k_{a4} + k_{a5} + k_{a6})[A_S]\frac{(\Psi R_{Max} - R^{\beta})}{M_w G}$$
$$+\frac{(k_{d4}R^{\beta Y} + k_{d5}R^{\beta Z} + k_{d6}R^{\beta X})}{M_w G}$$
$$-(k_{a1} + k_{a2} + k_{a3} + k_{a4} + k_{a5} + k_{a6})[A_S]\frac{(\Omega R_{Max} - R_{2P}^{1\times Docked} - R^{\alpha\beta})}{M_w G}$$
$$+\frac{(k_{d1}R_{2P}^{\alpha X} + k_{d2}R_{2P}^{\alpha Y} + k_{d3}R_{2P}^{\alpha Z} + k_{d4}R_{2P}^{\beta Y} + k_{d5}R_{2P}^{\beta Z} + k_{d6}R_{2P}^{\beta X})}{M_w G})/h_d \quad (4.1)$$

$$dR^{\alpha X}/dt = k_{a1}[A_S](\Pi R_{Max} - R^{\alpha}) - k_{d1}R^{\alpha X} \quad (4.2)$$

$$dR^{\alpha Y}/dt = k_{a2}[A_S](\Pi R_{Max} - R^{\alpha}) - k_{d2}R^{\alpha Y} \tag{4.3}$$

$$dR^{\alpha Z}/dt = k_{a3}[A_S](\Pi R_{Max} - R^{\alpha}) - k_{d3}R^{\alpha Z} \tag{4.4}$$

$$\frac{dR^{\alpha}}{dt} = \frac{dR^{\alpha X}}{dt} + \frac{dR^{\alpha Y}}{dt} + \frac{dR^{\alpha Z}}{dt} \tag{4.5}$$

$$dR^{\beta Y}/dt = k_{a4}[A_S](\Psi R_{Max} - R^{\beta}) - k_{d4}R^{\beta Y} \tag{4.6}$$

$$dR^{\beta Z}/dt = k_{a5}[A_S](\Psi R_{Max} - R^{\beta}) - k_{d5}R^{\beta Z} \tag{4.7}$$

$$dR^{\beta X}/dt = k_{a6}[A_S](\Psi R_{Max} - R^{\beta}) - k_{d6}R^{\beta X} \tag{4.8}$$

$$\frac{dR^{\beta}}{dt} = \frac{dR^{\beta X}}{dt} + \frac{dR^{\beta Y}}{dt} + \frac{dR^{\beta Z}}{dt} \tag{4.9}$$

$$\frac{dR_{2P}^{\alpha X}}{dt} = k_{a1}[A_S](\Omega R_{Max} - R_{2p}^{1\times Docked} - R^{\alpha\beta})$$
$$-(k_{d1} + k_{a4}^{\star\star} + k_{a5}^{\star})R_{2P}^{\alpha X} + k_{d4}R^{\alpha X\beta Y} + k_{d5}R^{\alpha X\beta Z} \tag{4.10}$$

$$\frac{dR_{2P}^{\alpha Y}}{dt} = k_{a2}[A_S](\Omega R_{Max} - R_{2p}^{1\times Docked} - R^{\alpha\beta})$$
$$-(k_{d2} + k_{a5}^{\star\star} + k_{a6}^{\star})R_{2P}^{\alpha X} + k_{d5}R^{\alpha X\beta Y} + k_{d6}R^{\alpha X\beta Z} \tag{4.11}$$

$$\frac{dR_{2P}^{\alpha Z}}{dt} = k_{a3}[A_S](\Omega R_{Max} - R_{2p}^{1\times Docked} - R^{\alpha\beta})$$
$$-(k_{d3} + k_{a4}^{\star} + k_{a6}^{\star\star})R_{2P}^{\alpha Z} + k_{d4}R^{\alpha Z\beta Y} + k_{d6}R^{\alpha Z\beta X} \tag{4.12}$$

$$\frac{dR_{2P}^{\beta Y}}{dt} = k_{a4}[A_S](\Omega R_{Max} - R_{2p}^{1\times Docked} - R^{\alpha\beta})$$
$$-(k_{d4} + k_{a1}^{\star\star} + k_{a3}^{\star})R_{2P}^{\beta Y} + k_{d1}R^{\alpha X\beta Y} + k_{d3}R^{\alpha Z\beta Y} \tag{4.13}$$

$$\frac{dR_{2P}^{\beta Z}}{dt} = k_{a5}[A_S](\Omega R_{Max} - R_{2p}^{1\times Docked} - R^{\alpha\beta})$$
$$-(k_{d5} + k_{a1}^{\star} + k_{a2}^{\star})R_{2P}^{\beta Z} + k_{d1}R^{\alpha X\beta Z} + k_{d2}R^{\alpha Y\beta Z} \tag{4.14}$$

$$\frac{dR_{2P}^{\beta X}}{dt} = k_{a6}[A_S](\Omega R_{Max} - R_{2p}^{1\times Docked} - R^{\alpha\beta})$$
$$-(k_{d6} + k_{a2}^{\star\star} + k_{a3}^{\star\star})R_{2P}^{\beta X} + k_{d2}R^{\alpha Y\beta X} + k_{d3}R^{\alpha Z\beta X} \tag{4.15}$$

$$\frac{dR_{2P}^{1\times Docked}}{dt} = \frac{dR_{2P}^{\alpha X}}{dt} + \frac{dR_{2P}^{\alpha Y}}{dt} + \frac{dR_{2P}^{\alpha Z}}{dt} + \frac{dR_{2P}^{\beta X}}{dt} + \frac{dR_{2P}^{\beta Y}}{dt} + \frac{dR_{2P}^{\beta Z}}{dt} \tag{4.16}$$

$$\frac{dR^{\alpha X\beta Y}}{dt} = k_{a1}^{\star\star} R_{2P}^{\beta Y} + k_{a4}^{\star\star} R_{2P}^{\alpha X} - (k_{d1} + k_{d4}) R^{\alpha X\beta Y} \tag{4.17}$$

$$\frac{dR^{\alpha X\beta Z}}{dt} = k_{a1}^{\star} R_{2P}^{\beta Z} + k_{a5}^{\star} R_{2P}^{\alpha X} - (k_{d1} + k_{d5}) R^{\alpha X\beta Z} \tag{4.18}$$

$$\frac{dR^{\alpha Y\beta Z}}{dt} = k_{a2}^{\star} R_{2P}^{\beta Z} + k_{a5}^{\star\star} R_{2P}^{\alpha Y} - (k_{d1} + k_{d5}) R^{\alpha Y\beta Z} \tag{4.19}$$

$$\frac{dR^{\alpha Y\beta X}}{dt} = k_{a2}^{\star\star} R_{2P}^{\beta X} + k_{a6}^{\star} R_{2P}^{\alpha Y} - (k_{d2} + k_{d6}) R^{\alpha Y\beta X} \tag{4.20}$$

$$\frac{dR^{\alpha Z\beta X}}{dt} = k_{a3}^{\star\star} R_{2P}^{\beta X} + k_{a6}^{\star\star} R_{2P}^{\alpha Z} - (k_{d3} + k_{d6}) R^{\alpha Z\beta X} \tag{4.21}$$

$$\frac{dR^{\alpha Z\beta Y}}{dt} = k_{a3}^{\star} R_{2P}^{\beta Y} + k_{a4}^{\star} R_{2P}^{\alpha Z} - (k_{d3} + k_{d4}) R^{\alpha Z\beta Y} \tag{4.22}$$

$$\begin{aligned}\frac{dR^{\alpha\beta}}{dt} &= \frac{dR^{\alpha X\beta Y}}{dt} + \frac{dR^{\alpha X\beta Z}}{dt} + \frac{dR^{\alpha Y\beta Z}}{dt} \\ &+ \frac{dR^{\alpha Y\beta X}}{dt} + \frac{dR^{\alpha Z\beta X}}{dt} + \frac{dR^{\alpha Z\beta Y}}{dt}\end{aligned} \tag{4.23}$$

$$\frac{dR_{Total}}{dt} = \frac{dR^{\alpha}}{dt} + \frac{dR^{\beta}}{dt} + \frac{dR_{2P}^{1\times Docked}}{dt} + \frac{dR^{\alpha\beta}}{dt} \tag{4.24}$$

2.7 Determination of kinetic constants

Data modification including scale transformation and background subtraction was performed with the program BIAevaluation 4.1. Data analyses and calculations based on numerical approaches, including global curve fitting to interaction models for estimation of kinetic constants, were performed with IGOR Pro (version 4.09.0, WaveMetrics, Inc.). Curve fit functions based on models 1, 2, 3, and 4 were created as external operation routines, compiled in C, using CodeWarrior IDE (version 5.1.1.1105, Metrowerks Corporation) and applied together with the Global Fit Procedure in IGOR Pro, based on a nonlinear least-squares method, utilizing the Levenberg-Marquard algorithm (Press et al., 1999). For numerical integration, a fifth order Runge-Kutta-Fehlberg method was applied (Press et al., 1999). Previous mathematical analysis has demonstrated that this numerical procedure, used in the curve fitting routine, gives precise and accurate solutions of the underlying differential equations (Sigmundsson et al., 2002).

2.8 Computational analysis of SHP-1 binding to mono- and di-phosphorylated CEACAM1-L

The kinetic rate constants determined by the BIAcore analyses were used to compute the binding kinetics of the SHP-1 tandem N,C-$(SH2)_2$ domain to CEACAM1-L phosphorylated on Y488 only, or on both Y488 and Y515. This was done by setting up complete reaction

schemes for all possible pathways leading to the reversible formation of all complexes that were identified by the experimental BIAcore analyses (see Tables 1 and 2 and Fig. 4C). The coupled, non-linear differential equations that were formulated from these reaction schemes were solved numerically, utilizing IGOR Pro.

3. Results

3.1 Interaction profiles

Interaction profiles of uncleaved and cleaved GST-fusion constructs of SHP-1 N-SH2, C-SH2, and N,C-$(SH)_2$ domains with biotinylated peptides were recorded at 25° C. The SH2 domains interacted specifically with the two phosphorylated ITIM-like peptide motifs, whereas responses with unphosphorylated ITIM-like sequences involving Y488 and Y515, and a scrambled Y488 sequence, were insignificant and resembled the background profiles of a ligand-free streptavidin surface (Fig. 2A-F). No binding was observed between GST and the ligand surfaces (Fig. 2H). The N-SH2, C-SH2 and N,C-$(SH2)_2$ domains all interacted with the pY488 ligand. However, the dissociation of the GST-fusion proteins was significantly slower compared with that of the GST-free N-SH2, C-SH2 and N,C-$(SH2)_2$ domains (blue curves in Figure 2: A vs. B, C vs. D, E vs. F). In fact, the binding of GST-C-SH2 and GST-N,C-$(SH2)_2$ to pY488 gave rise to severe difficulties in regeneration of the ligand surface. These results indicate that the GST moiety caused secondary interactions between the analyte molecules at the surface.

No interaction was detected between pY515 and GST-N-SH2 or the N-SH2 domain (Fig. 2A-B: red curves). The GST-C-SH2 and GST-N,C-$(SH2)_2$ proteins gave minor responses with the pY515 ligand, while the free C-SH2 and N,C-$(SH2)_2$ domains showed significant interaction (Fig. 2C-F: red curves). These results indicate that the GST part of these fusion proteins blocked the access to a pY515 interaction site, which became available for binding in the GST-free C-SH2 and N,C-$(SH2)_2$ domains. Together, Figures 2C and 2D indicate that the C-SH2 domain holds 2 different binding sites. One of these is accessible (C1-site) and the other is blocked (C2-site) in the GST-C-SH2 form. The accessible C1-site interacts with the pY488 ligand (blue), while the response to pY515 (red) is minimal (Fig. 2C). The C2-site on the C-SH2 domain becomes accessible after cleavage from the GST fusion partner (Fig. 2D), giving a characteristic binding profile to the pY515 ligand (red). This same site gives rise to an additional profile in response to the pY488 ligand (blue), characterized by a sharp change in the start of the association and dissociation phases (marked by arrows in Fig. 2D). The same blockage of interaction with pY515 was seen for the GST-N,C-$(SH2)_2$ protein (Fig. 2E) when compared with the response patterns of free N,C-$(SH2)_2$ (Fig. 2F). Figure 2G shows an interaction with the anti-phosphotyrosine antibody (PY99), confirming identical immobilization levels for the pY488 (blue) and pY515 (red) ligands.

3.2 Determination of kinetic constants for SH2 domains binding to distinct phosphotyrosine ligands

Due to high avidity and problems with surface regeneration, it was not possible to collect data for kinetic evaluation of the interactions of GST-C-SH2 and GST-N,C-$(SH2)_2$ with the biotinylated pY488 and pY515 ligands. Furthermore, the interaction of GST-N-SH2 with the biotinylated pY488 peptide could not be evaluated by any simple interaction models. The free N-SH2 and C-SH2 domains were also unsuitable for kinetic analysis because they underwent slow inactivation after cleavage of the GST moiety. Thrombin cleavage of the GST-N,C-$(SH2)_2$ protein on the other hand provided a stable N,C-$(SH2)_2$ tandem domain,

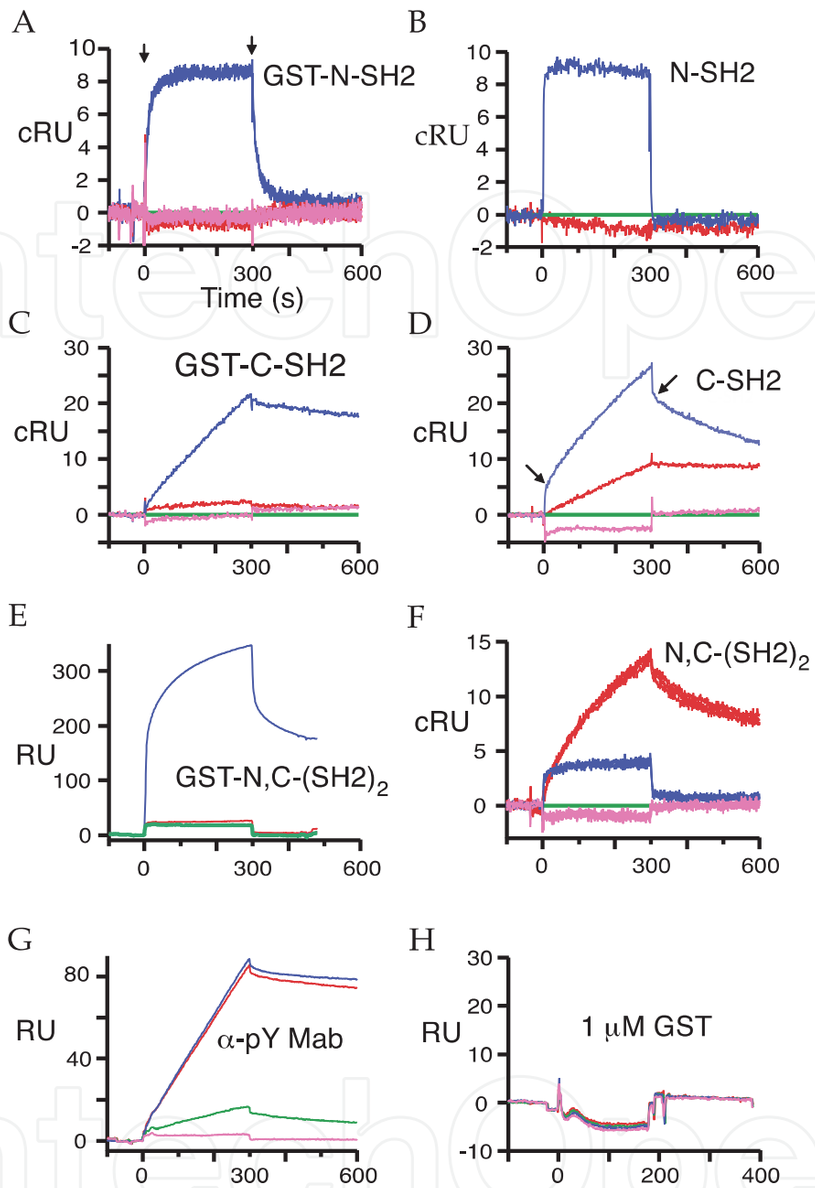

Fig. 2. Sensorgrams showing interaction profiles for SH2 domains derived from SHP-1 (non-cleaved and cleaved from GST). Responses to the different CEACAM1-L-derived biotinylated peptide ligands have the following colours: pY488 = blue, pY515 = red, Y488 = green (reference lane) and a free streptavidin surface = pink. Analyte: A) GST-N-SH2, 2 nM (3 × repeat), arrows indicate the start and end of sample injection. B) N-SH2, 4 nM. C) GST-C-SH2, 10 nM. D) C-SH2, 15 nM, arrows indicate the two different profiles seen in the start of the association and dissociation phases. E) GST-N,C-$(SH2)_2$, 15 nM. F) N,C-$(SH2)_2$, 20 nM (3 × repeat). G) PY99 Mab, 1 nM. H) GST, 1 µM. RU: Response units, cRU: corrected response units (response from the reference lane has been subtracted). Measurements were performed in HBS, pH 7.4, 25˚ C, at a flow of 20 µl/min. Low density ligand surfaces were used in A, B, C, D, F, G, H. A high density ligand surface was used in E.

which could be used for kinetic interaction analysis. For this purpose we used ligand surfaces with N-terminally cysteinylated peptides, to circumvent the regeneration problems with the biotinylated peptide ligands. Recordings at five different temperatures showed that the interactions of N,C-$(SH2)_2$ with the pY488 and pY515 motifs were strongly temperature-dependent, exhibiting an overall increase in both association and dissociation rates with increasing temperature (Fig. 3). However, the interaction patterns were complex and could not be fitted to the simple interaction model 1, or to a two-state version of model 1 in which the primary binding is followed by a more stable binding (not shown). Thus, in order to work out the kinetics, we designed and applied fit routines based on plausible interaction paths and the information obtained from the experiments described in Figure 2. These routines were denoted models 2 and 3. The resulting curve fittings are shown in Figure 3, and the respective rate constants from these fits are listed in Table 1. Using these rate constants, the curve fit for the highest concentration of each data set (plotted red) was subjected to profile analysis of the underlying, contributing binding reactions (plotted black, blue and green), as shown in Figure 3. In addition, we estimated the surface-to-bulk analyte concentration ratio ($[A_{surface}]/[A_{bulk}]$) during the interval of sample injection, by applying the same parameters and rate constants as used and obtained in the fit approaches. These profiles (not shown) indicated the data recordings to be essentially free of mass transport limitation.

Recordings of the interaction of N,C-$(SH2)_2$ with the pY488 motif indicated some higher degree of complexity. At 5° and 15° C model 3 matched best with this interaction, whereas applying model 3 at 25° and 35° C, resulted in a reduction to model 2. Similarly, at 37° C the interaction was best described by model 2, although a reduction towards model 1 was indicated. The profile that contributed the most to the total signal at all temperatures was the N-SH2-site interacting with the pY488 motif (Fig. 3, black dashed curve). This interaction is characterized by rapid association and dissociation (Table 1; see also Figs. 2A and B). Competition from one or two additional binding sites on the N,C-$(SH2)_2$ protein (belonging to the C-SH2 domain) leads to slight profile changes. In the inserted graph in Figure 3 at 25° C (black: N-SH2 site binding to pY488), we demonstrate with a simulation based on the observed rate constants, how the profile for the N,C-$(SH2)_2$ molecule would appear if only the N-SH2 site was active, and the other binding sites were inactive. The similarity of this profile with that observed for the isolated N-SH2 domain in Figure 2B is striking. From comparison with the binding profiles of the single SH2 domains (Figs. 2A-D) we conclude that the second binding reaction, plotted as green dashed profiles in Fig. 3 (left panels), represents the C1-SH2 site interaction with the pY488 motif. This interaction showed slow association and dissociation, resembling the observed binding profile for the interaction of the GST-C-SH2 accessible site with pY488 (Figs. 2C and D, blue curves). Interestingly, this interaction was most pronounced at 25° C and decreased with further rise in temperature, and therefore appears to be less relevant at physiological temperature (37° C). The third binding reaction (blue dashed profiles in Fig. 3, left panels) corresponded to the interaction of pY488 with the C2-SH2 site (the inaccessible site in GST-C-SH2, according to Fig. 2C and D, which is the part of the blue curve characterized by a fast on/off profile, indicated by arrows in Fig 2D). This interaction was also highly temperature-dependent. From 15° to 25° C its magnitude decreased markedly, and at temperatures ≥ 35° C it no longer existed. This is shown in Figure 3, where the data recorded at 25° and 35° C were analyzed with a function based on model 3 (returning an infinitely small k_{a3}). It should be pointed out that in contrast to the results displayed in Figure 3, Figure 2D shows that the C2-site of the isolated C-SH2 domain interacted with the pY488 ligand at 25° C, and provided a minor but detectable contribution to the recorded signal. Thus, this interaction might only occur for the

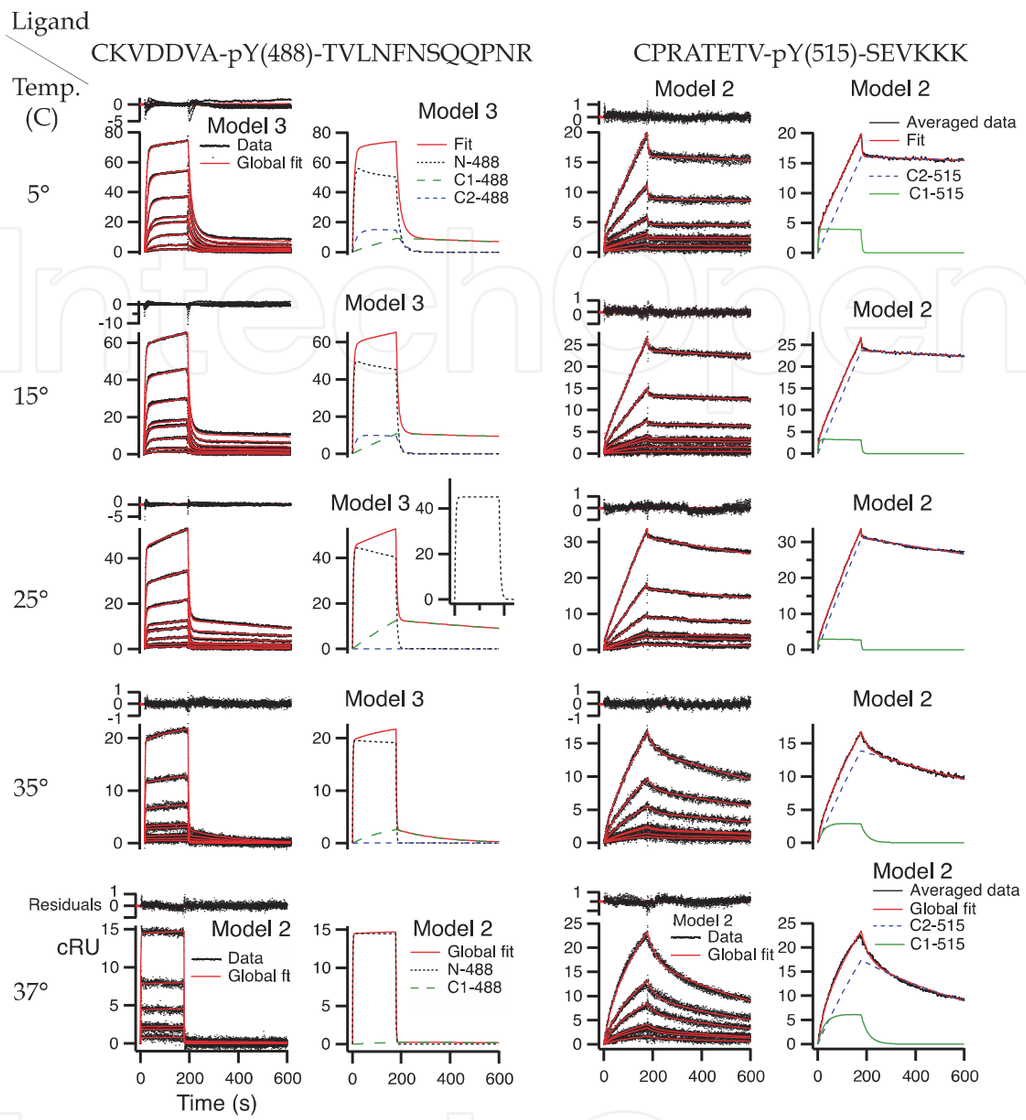

Fig. 3. Sensorgrams for the interactions of N,C-$(SH2)_2$ with the CEACAM1-L-derived cysteinylated phosphopeptides pY488 (left panel) and pY515 (right panel), at various temperatures. At each temperature samples were injected for 3 minutes in a randomized order with a total of three injections per concentration. All data are shown (black) together with global curve fits (red). Residuals are shown above each global fit result. For the pY488 ligand at 5°, 15°, 25° and 35°, fits were based on model 3. Fits for pY488 at 37° and for pY515 at all temperatures, were based on model 2. Analyte concentrations were defined as fit variables, with the initial values of 120, 60, 30, 15, 12, 6, 3, and 1.5 nM, as estimated from dilution factors and applied with constraints of ± 30 %, in global fit approaches. Flow rate was 20 µl/min. R_{Max} was 120 and 510 RU for the pY488 and pY515 surfaces, respectively. For the 24.9 kDa analyte, diffusion coefficients and h_d at 5°, 15°, 25°, 35° and 37° C were: (9.5, 9.8, 10.2, 10.5, 10.6)×10^{-7} cm^2s^{-1}, and 6.84, 6.92, 7.00, 7.08, 7.10 µm, respectively. Profile analysis for the 120 nM concentration responses is provided to the right of each fit panel. cRU: corrected response units. The results are tabulated in Table 1.

isolated C-SH2 domain at 25° C and above, disappearing in the N,C-$(SH2)_2$ domain for conformational/stability reasons.

At 37° C the interaction of the C1-SH2 site with pY488 also disappeared almost completely. The decrease in binding of the C1-SH2 and C2-SH2 sites to pY488 with increasing temperature represents a true temperature-dependence and was not caused by denaturation of the C-SH2 domain, since both of these sites bound significantly to pY515, even at 37° C (Fig. 3, right panels; Table 1). Thus, at 37° C, the interaction of the N,C-$(SH2)_2$ tandem domain with pY488 approached model 1, in which the rapid association/dissociation between the N-SH2 domain and the pY488 motif dominated.

The analysis of the N,C-$(SH2)_2$ binding to the pY515 peptide gave excellent curve fittings applying model 2, at all temperatures. From the data shown in Figures 2A and B (red curves), we know that the N-SH2 domain did not interact with pY515. Therefore, it is unlikely that the N-SH2 domain was involved in the interaction of N,C-$(SH2)_2$ with pY515. Accordingly, and by comparing with the binding profiles of the single SH2 domains (Figs. 2C-F), we refer to the major reaction of the N,C-$(SH2)_2$ with pY515 (Fig. 3, right panels: blue dashed profile) as the C2- site, i.e. the GST-C-SH2-inaccessible site in the pY515 interaction (Fig. 2 C,D: red profiles). The less pronounced reaction (Fig.3: green profiles) we refer to as the C1-SH2 site, i.e. the GST-C-SH2 accessible site in the interaction with pY515. While the interaction of the C1-SH2 site with pY515 appears minimal at 25° C, it becomes significant at 35° and 37° C.

Interaction	Temp	k_a	k_d	K_d
	°C	$M^{-1}\ s^{-1}$	s^{-1}	M
N-SH2:pY488	5	$1.45\times10^{6}\pm1.6\times10^{5}$	$1.0\times10^{-1}\pm 5\times10^{-3}$	7.4×10^{-8}
	15	$1.72\times10^{6}\pm3.6\times10^{5}$	$2.3\times10^{-1}\pm2\times10^{-2}$	1.4×10^{-7}
	25	$1.83\times10^{6}\pm1.6\times10^{4}$	$3.2\times10^{-1}\pm3\times10^{-3}$	1.8×10^{-7}
	35	$2.00\times10^{6}\pm1.5\times10^{2}$	$9.9\times10^{-1}\pm1\times10^{-3}$	5.0×10^{-7}
	37	$2.17\times10^{6}\pm1.7\times10^{5}$	$1.5\ \pm5\times10^{-2}$	6.9×10^{-7}
C1-SH2:pY488	5	$1.37\times10^{4}\pm9.8\times10^{2}$	$7.1\times10^{-4}\pm6\times10^{-5}$	5.2×10^{-8}
	15	$9.48\times10^{3}\pm1.3\times10^{3}$	$3.5\times10^{-4}\pm3\times10^{-5}$	3.7×10^{-8}
	25	$1.01\times10^{4}\pm0.6\times10^{1}$	$8.0\times10^{-4}\pm1\times10^{-5}$	7.9×10^{-8}
	35	$2.33\times10^{3}\pm3.6\times10^{1}$	$5.5\times10^{-3}\pm8\times10^{-5}$	2.4×10^{-6}
	37	$1.39\times10^{2}\pm1.8\times10^{1}$	$3.8\times10^{-4}\pm2\times10^{-4}$	2.8×10^{-6}
C2-SH2:pY488	5	$1.52\times10^{5}\pm5.1\times10^{4}$	$3.9\times10^{-2}\pm5\times10^{-3}$	2.6×10^{-7}
	15	$1.00\times10^{5}\pm4.0\times10^{3}$	$7.0\times10^{-2}\pm1\times10^{-2}$	6.5×10^{-7}
C1-SH2:pY515	5	$2.54\times10^{4}\pm1.8\times10^{3}$	$2.9\times10^{-1}\pm9\times10^{-3}$	1.1×10^{-5}
	15	$1.86\times10^{4}\pm1.0\times10^{3}$	$2.6\times10^{-1}\pm1\times10^{-2}$	1.4×10^{-5}
	25	$2.18\times10^{4}\pm4.1\times10^{3}$	$4.2\times10^{-1}\pm3\times10^{-2}$	2.1×10^{-5}
	35	$2.68\times10^{3}\pm5.0\times10^{1}$	$4.2\times10^{-2}\pm1\times10^{-3}$	1.6×10^{-5}
	37	$3.98\times10^{3}\pm6.3\times10^{1}$	$3.5\times10^{-2}\pm6\times10^{-4}$	8.8×10^{-6}
C2-SH2:pY515	5	$1.95\times10^{3}\pm1.3\times10^{2}$	$9.4\times10^{-5}\pm4\times10^{-6}$	4.8×10^{-8}
	15	$2.94\times10^{3}\pm1.2\times10^{2}$	$1.43\times10^{-4}\pm3\times10^{-6}$	4.9×10^{-8}
	25	$3.25\times10^{3}\pm6.0\times10^{2}$	$3.72\times10^{-4}\pm3\times10^{-6}$	1.2×10^{-7}
	35	$1.83\times10^{3}\pm5.0\times10^{1}$	$9.01\times10^{-4}\pm 8\times10^{-6}$	4.9×10^{-7}
	37	$2.08\times10^{3}\pm1.4\times10^{1}$	$1.58\times10^{-3}\pm1\times10^{-5}$	7.6×10^{-7}

Table 1. Kinetic parameters for the interactions between the SHP-1 N,C-$(SH2)_2$ domain and CEACAM1-L derived pY488 and pY515 peptides.

3.3 Determination of the mechanism and kinetic constants for the interaction of the N,C-$(SH2)_2$ domain with the CEACAM1-Lcyt cytoplasmic domain

Finally, we analyzed the interaction at 25˚ C of the tandem N,C-$(SH2)_2$ domain with the full size cytoplasmic domain of CEACAM1-L, phosphorylated on both tyrosine residues (Y488 and Y515). According to mass spectrometry analysis c:a 75% of the GST-Lcyt ligand, produced in the *E. coli* TKX1 strain, was phosphorylated. Approximately 34% of the phosphorylated fraction was accounted for by di-phosphorylated GST-Lcyt (pY488, pY515), 63 % was mono-phosphorylated on Y488, and c:a 3 % was mono-phosphorylated on Y515. The phosphorylated GST-Lcyt ligand (34.2 kDa) was immobilized to give 112 RU. This provided a theoretical R_{Max} of c:a 115 RU with respect to N,C-$(SH2)_2$ (24.9 kDa) binding, assuming a binding ratio of 1:1 and 100% ligand access. The N,C-$(SH2)_2$ domain showed no detectable interaction with the GST reference surface.

		Ligand			
		CEACAM1-L cytoplasmic domain		pY-peptide	
Parameter	Fixed	Value	± SD	Value	Interaction
k_{a1} ($M^{-1}s^{-1}$)	●	1.83×10^{6}		1.83×10^{6}	N-SH2 to pY488
k_{d1} (s^{-1})		2.69×10^{-1}	3.7×10^{-3}	3.20×10^{-1}	N-SH2 off pY488
k_{a2} ($M^{-1}s^{-1}$)	●	0		Negligible	C2-SH2 to pY488
k_{d2} (s^{-1})	●	0		Negligible	C2-SH2 off pY488
k_{a3} ($M^{-1}s^{-1}$)	●	1.01×10^{4}		1.01×10^{4}	C1-SH2 to pY488
k_{d3} (s^{-1})	●	8.00×10^{-4}		8.00×10^{-4}	C1-SH2 off pY488
k_{a4} ($M^{-1}s^{-1}$)	●	3.25×10^{3}		3.25×10^{3}	C2-SH2 to pY515
k_{d4} (s^{-1})	●	3.72×10^{-4}		3.72×10^{-4}	C2-SH2 off pY515
k_{a5} ($M^{-1}s^{-1}$)	●	2.18×10^{4}		2.18×10^{4}	C1-SH2 to pY515
k_{d5} (s^{-1})		2.32×10^{-2}	1.4×10^{-3}	4.20×10^{-1}	C1-SH2 off pY515
k_{a1*} (s^{-1}) *i)*		0.35	0.12		N-SH2 to pY488 on C1-SH2:pY515
k_{a5*} (s^{-1}) *i)*		4.81	0.14		C1-SH2 to pY515 on N-SH2:pY488
k_{a1*} (s^{-1}) *ii)*		3.94	2.19		N-SH2 to pY488 on C1-SH2:pY515
k_{a5*} (s^{-1}) *ii)*		0.50	0.02		C1-SH2 to pY515 on N-SH2:pY488

Table 2. Kinetic parameters for the interaction between the SHP-1 N,C-$(SH2)_2$ domain and the tyrosine-phosphorylated CEACAM1-L cytoplasmic domain. The experimental data shown in Figure 4A were analyzed by Model 4. The kinetic parameters are defined in Model 4. The parameters labelled (●) were kept fixed during the curve fitting runs. The parameter values for the pY-peptide ligand were taken from Table 1.

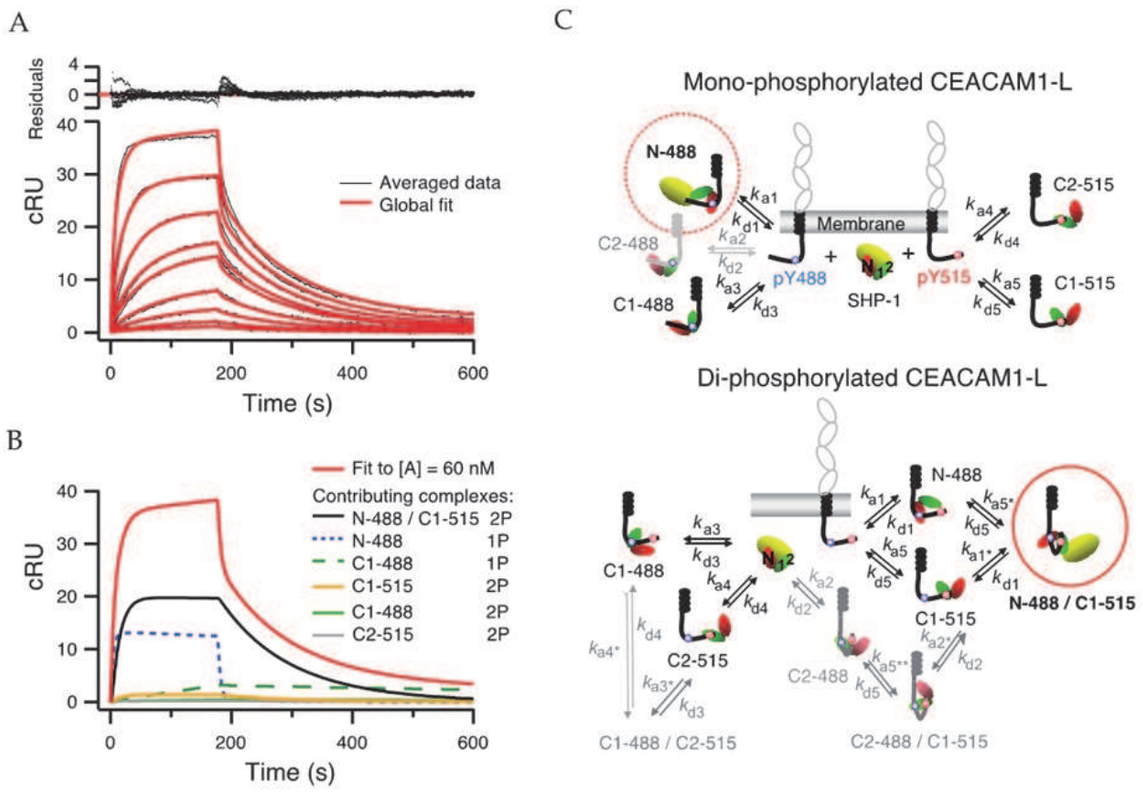

Fig. 4. The interaction of N,C-$(SH2)_2$ with mono- and di-phosphorylated CEACAM1-L cytoplasmic domain. The N,C-$(SH2)_2$ domain of SHP-1 was injected at 25° C for 3 min, at 20 µl/min. Ligand with the composition of 63 % GST-Lcyt-pY488, 3 % GST-Lcyt-pY515 and 34 % GST-Lcyt-[pY488/pY515], according to mass spectrometry analysis, was immobilized (112 RU) on a low density anti-GST-Ab surface. Reference surface was saturated with GST. A) Sensorgram showing averaged responses of three runs per concentration (black) of 60, 30, 15, 12, 6, 3, 1.5, 0.75, 0.375 nM, together with a global curve fit (red), based on an optimized interaction model described in C. The averaged squared residual per data point, $\overline{r}^{\,2}$, was 0.188. The results are tabulated in Table 2. B) Profile analysis showing the contribution of the different complex forms to the response obtained at [Analyte] = 60 nM. Complexes are indicated with N-488/C1-515: N-SH2 bound to pY488 and C1-SH2 bound to pY515 in tandem; N-488: N-SH2 bound to pY488; C1-488: C1-SH2 bound to pY488; C1-515: C1-SH2 bound to pY515; C2-515: C2-SH2 bound to pY515. The tyrosine-phosphorylation status of the ligand in a particular complex is indicated by 1P and 2P, for mono- and di-phosphorylation, respectively. C) A scheme for the interactions predicted by the global fit results in A. The N-SH2 domain is coloured red, the C-SH2 domain is coloured green, and the phosphatase domain is coloured yellow. For simplicity reasons the phosphatase domain (yellow) was omitted from all but two complexes, and the CEACAM1 extracellular domain (grey) is only shown on the non-complexed molecules. Interactions suggested by the global fit-results are indicated in black. Interactions excluded by the fit results are indicated in grey. Red circles are drawn around the most ubiquitous complexes (dashed circle for a mono-phosphorylated ligand and solid circle for a di-phosphorylated ligand).

A special curve fit approach was designed for an interaction model which allowed testing of all combinations of single and double dockings (model 4). Constraints were introduced to exclude non-permissible interactions, such as N-SH2 interactions with pY515. Initial values for confirmed interactions were obtained from Table 1 and the number of fit parameters and variables were trimmed to a minimum. Despite our efforts to provide various initial values for the pY488 binding to the C2-site (represented in our model by k_{a2}), the fit-routine consistently repressed this parameter to zero, indicating a non-existant or irrelevant interaction, in agreement with the results obtained with the mono-phosphorylated pY488 peptide (Table 1). This eliminated two variables (k_{a2} and k_{d2}) from the model. Likewise, all forms of double-docked complexes could be eliminated except the N-488/C1-515, which was mandatory for adequate quality fit results. According to this analysis, a total of five complexes were formed. Four of these belonged to the single-docked forms, observed earlier on the mono-phosphorylated peptide surfaces at 25° C. The fifth form was the double-docked N-488/C1-515 complex. The results from this analysis are shown in Figure 4 and tabulated in Table 2. Importantly, the primary rate constants diverged minimally from those obtained with the mono-phosphorylated peptides. However, the results included two indistinguishable solutions for the secondary rate constants, k_{a1^*} and k_{a5^*}, which describe the second docking event, during the formation of a double-docked complex (Fig. 4C). Both solutions are listed in Table 2, labelled with superscripts: $^{i)}$ $k_{a1^*} < k_{a5^*}$ and $^{ii)}$ $k_{a1^*} > k_{a5^*}$. Although the fit approach could not distinguish between these two solutions, it seems logical that the second alternative, $k_{a1^*} > k_{a5^*}$, is more probable, because the corresponding primary rate constants showed the relation $k_{a1} >> k_{a5}$ for all conditions (Table 1). A profile analysis is provided in Fig. 4B. According to this result the most pronounced complex was the double-docked form with the N-SH2 site bound to pY488 and the C1-SH2 site bound to pY515. Complexes with two analyte molecules bound per di-pY-ligand were rejected by all fit algorithms. Such complexes probably do not form for steric reasons. The interaction model that satisfied the global curve fit result is schematized in Figure 4C.

3.4 Kinetics of the binding of the N,C-$(SH2)_2$ domain to mono- and di-phosphorylated CEACAM1-L

We wanted to determine both the kinetics and the equilibrium of all the types of complexes that SHP-1 could form with the CEACAM1-L cytoplasmic domain, either mono-phosphorylated on Y488, or fully di-phosphorylated on both Y488 and Y515. This could not be done by direct BIAcore experiments because experimental phosphorylation of the recombinant CEACAM1-L cytoplasmic domain always resulted in a mixture of mono- and di-phosphorylated protein. Therefore, we applied computational analysis utilizing the rate constant values from Table 2 for the 25° C condition. At 37° C, a compromise solution was applied, since experimental data did not exist for k_{a1^*} and k_{a5^*}. Primary rate constants from Table 1 for 37° C were thus applied together with the $^{ii)}$ $k_{a1^*} > k_{a5^*}$ values of Table 2. The computation was done for a reaction volume that consists of a shell including the lipid bilayer contained within a 20 nm thick extracellular layer and a 15 nm thick intracellular layer (Öbrink et al., 2002). CEACAM1 is anchored in the lipid bilayer, and based on earlier biochemical data we assumed the concentration of CEACAM1-L in the reaction volume to be 1.0 μM. An overall cellular concentration of SHP-1 was determined to 1.84 μM in cultured epithelial cells (unpublished results). This concentration value was kept constant during the computation, assuming non-limiting diffusion of SHP-1 from the inner bulk cytoplasmic region to the 15 nm thick cytoplasmic reaction volume. The results are displayed in Figure 5.

For CEACAM1-L mono-phosphorylated on Y488 the temperature is an essential factor, affecting which type of complex will govern the system (Fig. 5A, C). At 25° C, the N-SH2:pY488 complex (N-488) dominated during the first eight minutes, but thereafter the C1-SH2:pY488 form (C1-488) became predominant. Equilibrium was reached in 40 minutes, with 31 % N-488 and 69 % C1-488. At 37° C, the N-488 complex dominated the system at all times, providing an opposite equilibrium of 80 % N-488 and 20 % C1-488.
The binding kinetics to CEACAM1-L phosphorylated on both Y488 and Y515 were somewhat more complex (Fig. 5B, D). Immediately after phosphorylation, the binding of the N-SH2 domain to pY488 accounted for c:a 80 % of total complexes. This complex then underwent a second docking to provide the double-docked N-488/C1-515 form. At both 25° and 37° C, the N-488/C1-515 form already dominated from the first minute and to equilibrium. At equilibrium at 37° C, N-488/C1-515 accounted for 62% of all complexes and the single-docked C1-515 form accounted for 24 %. The single-docked N-488 and C2-515 forms accounted for c:a 6 % each. These results indicate the N-488 complex and the N-488/C1-515 complex to be the biologically relevant forms.

4. Discussion

The impetus for this work was to advance our understanding of the signaling by the cell adhesion molecule CEACAM1-L. Because of the central role of SHP-1 in CEACAM1-L-mediated signaling, we chose to initiate this line of studies with a thorough analysis of the binding interactions between SHP-1 and the CEACAM1-L tyrosine-phosphorylated cytoplasmic domain. We applied a surface plasmon resonance-based technique (the BIAcore flow cell biosensor) to investigate the key patterns and kinetics of the binding interactions of SHP-1 with CEACAM1-L. Because CEACAM1-L has two phosphotyrosine binding motifs and SHP-1 has two SH2 domains, there is potential for several combinations of simultaneously forming binding complexes. To analyze such a combinatorial system we applied a classical reductionistic approach, starting by characterizing interactions between single binding sites. Results from these analyses were then used as building blocks for more elaborate analyses of the interactions of the tandem N,C-$(SH2)_2$ domain of SHP-1 with the CEACAM1-L double-tyrosine-phosphorylated cytoplasmic domain.
Initially, we used GST-fusion proteins of the SHP-1 SH2 domains. An unforeseen complication with this approach was that the GST moiety blocked some binding sites in both the GST-C-SH2 and the GST-N,C-$(SH2)_2$ proteins, which was discovered when the GST moiety was cleaved from the fusion proteins. However, this blocking effect had a positive consequence, because it led to the discovery of an additional binding site for phosphotyrosine motifs in the C-SH2 domain. Thus, there are three binding sites for tyrosine-phosphorylated CEACAM1-L in the SH2 domains of SHP-1. Finding a third phosphotyrosine recognition site was not anticipated, but was a consequence of the unique detectability of the SPR-based approach, which demonstrates one of the advantages of our strategy and the novel algorithms for binding analysis.
Most SH2 domains are believed to have one binding site for phosphotyrosine motifs, involving ArgαA2 and ArgβB5 (Waksman et al., 1993). However, our finding of an additional binding site for phosphotyrosine in the C-SH2 domain of SHP-1 is supported by the work of Weber et al. (Weber et al., 2000). By detailed NMR analysis of a doubly tyrosine-phosphorylated peptide (from the polyoma middle T antigen) complexed with the N-SH2 domain of the p85 subunit of phosphoinositide 3-kinase, they found a second site, in which

the phosphotyrosine is coordinated by a network of hydrogen bonds with the three amino acids, E411, S412 and the ε-amino group of K423. Sequence alignment of the p85 N-SH2 domain with the C-SH2 domain of SHP-1 demonstrates that the latter has two lysine residues, K198 and K199 (Yang et al., 2003), in the positions corresponding to E411 and S412 in the former one. Thus, this region of the SHP-1 C-SH2 domain has two positively charged amino acids, which could interact with the CEACAM1-L negatively charged phosphotyrosine residues. Site localization and further characterization of the two phosphotyrosine binding sites in the SHP-1 C-terminal SH2 domain require structural analysis of co-crystals of SHP-1 SH2 domains with mono- and double-phosphorylated CEACAM1-L cytoplasmic domains.

Experiments with single SH2 domains binding to mono-phosphotyrosine peptides showed that some interactions, e.g. the binding of the N-SH2 domain to the pY488 motif, had very rapid association and dissociation phases. Because of the relatively small number of reading points in such phases, the curve fit algorithm could not distinguish between several sets of solutions for k_a and k_d. This called for constraints to be introduced in the curve fitting procedure. To that end we assumed that the combination of the smallest possible rate constants, which satisfied the curve fitting, represented the most accurate description of these fast reactions.

Because single N-SH2 and C-SH2 domains were unstable we performed all detailed kinetic analyses with the N,C-$(SH2)_2$ protein. The interactions of N,C-$(SH2)_2$ with the pY488 and pY515 peptides followed the binding profiles and patterns predicted by the binding interactions of the individual N-SH2 and C-SH2 domains (see Figs. 2 and 3). The design and utilization of appropriate interaction schemes (models 2 and 3) were thus straightforward. Kinetic analysis at several different temperatures, analyzed by models 2 and 3, confirmed the existence of two binding sites in the C-SH2 domain, and one binding site in the N-SH2 domain. However, the different binding interactions had different temperature-dependencies. The interaction of the C2-SH2 site with the pY488 motif, which according to our analysis was significant at and below 15° C, no longer existed at and above 25° C. Similarly, the interaction of the C1-SH2 site with the pY488 motif had a fairly slow dissociation rate at all tested temperatures, but its association rate decreased by two orders of magnitude, upon temperature change from 5° to 37° C. Thus, at 37° C the contribution of this interaction was markedly decreased. In contrast, the interaction of the C1-SH2 site with the pY515 motif, which barely was detectable at 25° C, became significant enough at 37° C to claim physiological relevance.

The kinetic binding properties of the different complexes between tyrosine-phosphorylated CEACAM1-L and SHP-1 lead to interesting conclusions about *in vivo* complex formation between these signaling proteins. In many cell types CEACAM1-L tyrosine-phosphorylation is transient, with a peak 5-10 minutes after the triggering event. Thus, binding of SH2 domain-containing tyrosine kinases and phosphatases to CEACAM1-L can only happen within this time span. Complexes characterized by rapid association, such as N-SH2 binding to the pY488 site, will dominate early after tyrosine-phosphorylation relative to complexes with similar equilibrium binding affinities but slower association and dissociation. Computational analysis of the binding data obtained with the double-tyrosine-phosphorylated CEACAM1-L cytoplasmic domain and the tandem N,C-$(SH2)_2$ domain provided interesting insights into the time-dependent formation of the various CEACAM1-L:SHP-1 complexes. One finding was that the binding of SHP-1 to CEACAM1-L mono-phosphorylated on Y488 and to CEACAM1-L phosporylated on both Y488 and Y515, was

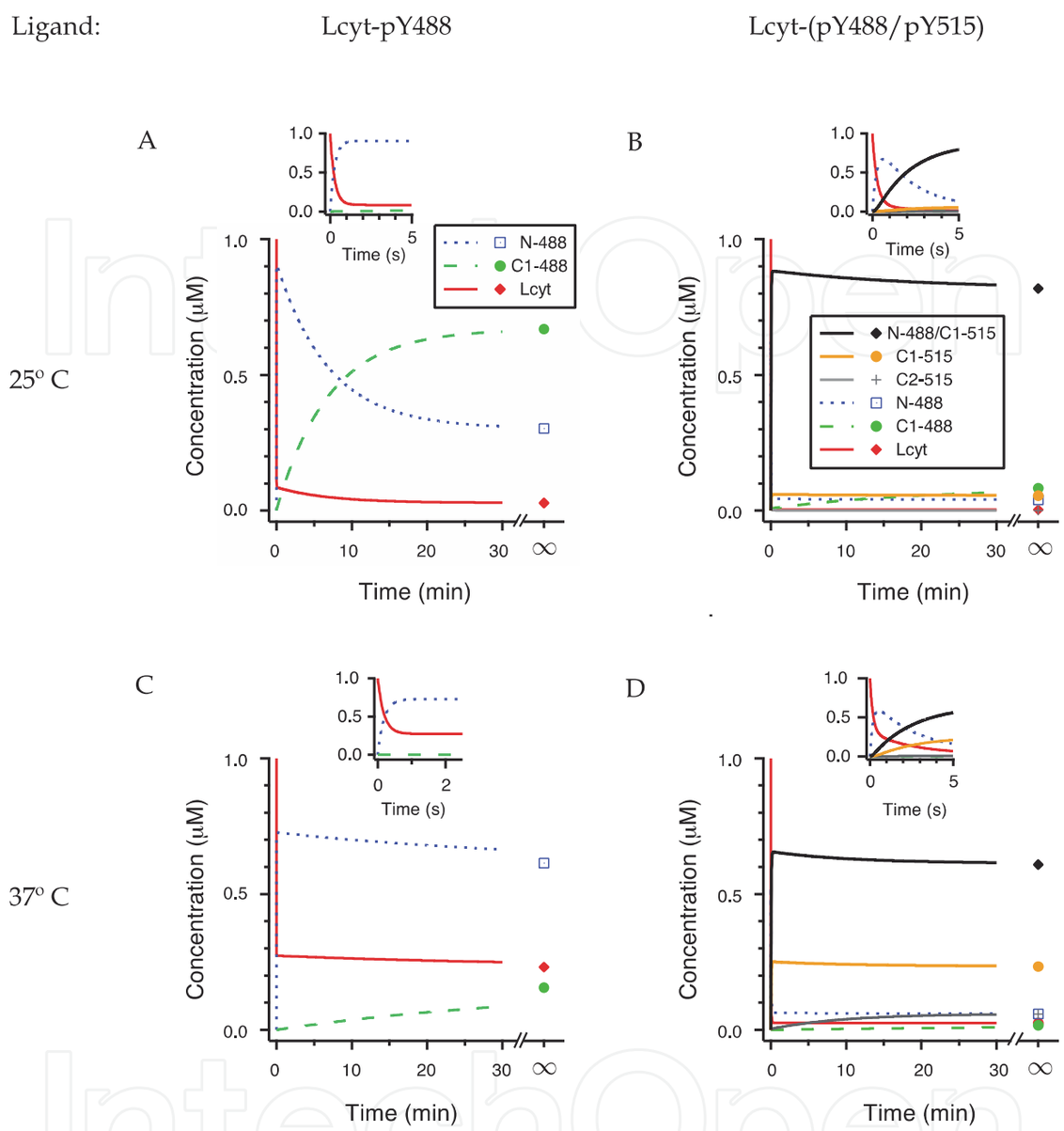

Fig. 5. Kinetics of the N,C-$(SH2)_2$ domain binding to mono- and di-phosphorylated CEACAM1-L. Interactions of CEACAM1-L mono-phosphorylated on Y488 (A,C) or di-phosphorylated on Y488 and Y515 (B,D), were analyzed computationally for two temperature conditions, 25° and 37° C, applying the model described in Fig. 4C. The initial membrane concentration of non-complexed phosphorylated CEACAM1-L was set to 1 μM; the cytoplasmic concentration of SHP-1 was kept constant, at 1.84 μM. For 25° C, the rate constants were taken from Table 2. For 37° C, the primary rate constants from Table 1 were used, together with k_{a1^*} [ii)] and k_{a5^*} [ii)] from Table 2. The notions provided in A are valid also for C. The notions provided in B are valid also for D. Complexes are indicated with N-488: N-SH2 bound to pY488; C1-488: C1-SH2 bound to pY488; C2-515: C2-SH2 bound to pY515; C1-515: C1-SH2 bound to pY515; N-488/C1-515: N-SH2 bound to pY488 and C1-SH2 bound to pY515 in tandem.

fairly similar. For CEACAM1-L mono-phosphorylated on Y488, binding of the N-SH2 domain dominated early after phosphorylation at 25° C (Fig. 5A), and at all times after phosphorylation at 37° C (Fig. 5C). At equilibrium the C1-SH2 site also contributed significantly. This binding pattern changed minimally for CEACAM1-L phosphorylated on both Y488 and Y515 (Fig. 5D). In this case the mono-docked N-488 complex dominated during the first few seconds, but gradually decreased as it served as a precursor for the double docked N-488/C1-515 complex, which became the dominant form (> 62 %) already within the first minute and ever after. The second most pronounced complex under these phosphorylation conditions was the mono-docked C1-515 form (24%).

It is believed that the N- and the C-SH2 domains have different functional roles in SHP-1, and that activation of the phosphatase is primarily due to engagement of the N-SH2 domain (Yang et al., 2003). Our data support this notion, and furthermore suggest that the role of the C-SH2 domain is primarily to stabilize the complex via engagement of the C1-SH2 site. Our data also suggests that phosphorylation of the membrane proximal tyrosine, Y488, in CEACAM1-L is the important reaction for activation of SHP-1, whereas phosphorylation of the distal tyrosine, Y515, primarily serves to stabilize the complex and sustain the activation state of the enzyme. This has functional implications, since it has been found that CEACAM1-L is preferentially phosphorylated on Y488 in some cell types, whereas in other cell types it becomes phosphorylated on both tyrosines (Brümmer et al., 1995; Huber et al., 1999). The transient versus stable CEACAM1-L tyrosine-phosphorylation also varies in different cell types. However, to fully understand the activation kinetics of SHP-1 it is necessary to also include CEACAM1-L's interactions with SHP-2 and c-Src, since these enzymes compete for the same binding sites in tyrosine-phosphorylated CEACAM1-L (Müller et al., 2009). Therefore, the kinetics and activation patterns of the binding of SHP-2 and c-Src to mono- and di-phosphorylated CEACAM1-L need to be investigated in future analyses.

The SPR-based approach is different from earlier approaches used to determine binding specificity and affinity of phosphopeptides to SH2 domains. In previous analyses, combinatorial libraries of short phosphopeptides have been used in pull-down assays, to characterize high affinity peptide sequence motifs for various SH2 domains (Songyang et al., 1993; Songyang et al., 1994). However, although providing optimal motifs with regard to stable binding, this method may not result in unbiased identification of physiologically relevant recognition motifs, since interactions dominated by slow dissociation rates are favored due to the obligatory washing steps included in the experimental procedures. Ligands with high dissociation rates, which will not be detected by the combinatorial peptide binding pull-down approach, may be of equally high affinity as ligands with slow dissociation, if they have fast association rates, since the equilibrium binding constant, K_d, equals the ratio k_d/k_a of the dissociation and association rate constants. Examples of binding reactions with similar equilibrium binding affinity, but with association and dissociation rates differing by three orders of magnitude are found in Table 1 (compare N-488 with C2-515). Such fast association/dissociation reactions, identified by our SPR-based procedure, may play very important roles in the control of signal cascades, because the resulting complexes will dominate early after tyrosine phosphorylation and will allow rapid switches between active and inactive enzyme states.

Finally, the interaction data presented in this paper (Figs. 3 and 5) emphasize that temperature is an important factor worth considering for all biochemical interactions. For various reasons, interaction studies involving mammalian proteins are routinely performed at temperatures considerably lower than physiological. Our data indicate that this can sometimes be misleading with regard to physiological relevance.

5. Conclusion

Signaling networks are at the heart of cellular functions in multicellular organisms. Such networks are composed of a large number of proteins that interact with each other in a complex and highly dynamic manner. Many of these interactions are characterized by rapid association/dissociation reactions between molecules having several distinct binding sites for each other. To initiate a deeper understanding of cell signaling we developed novel tools for characterizing the kinetics of macromolecules interacting through several distinct binding sites. This approach was based on utilization of SPR-based flow cell biosensors. It comprised a reductionistic approach starting with simple binding site interactions moving to molecules with multiple binding sites, and the development of novel algorithms for curve fitting analysis. By this approach we demonstrated that it is possible to make detailed analyses of the binding kinetics between macromolecules having 2-3 distinct binding sites for each other. We applied it to characterize the interactions of the signal regulating cell adhesion molecule CEACAM1-L with the protein tyrosine phosphatase SHP-1. Several new discoveries, with important implications for cell-cell recognition-mediated regulation of cellular signaling, were made. A novel binding site for phosphotyrosine-based motifs was discovered in the C-teminal SH2 domain in SHP-1. Some of the binding interactions were strongly temperature dependent, and disappeared at 37°C. This showed which of the binding interactions that are physiologically important. The detailed kinetic characterization together with computational analysis made it possible to determine the different roles of both the two tyrosine residues in the cytoplasmic domain of CEACAM1-L and of the two SH2 domains in SHP-1. Engagement of the N-terminal SHP-1 SH2 domain with the membrane proximal CEACAM1-L phosphotyrosine motif proved to be the most important interaction, whereas the C-terminal SHP-1 SH2 domain and the membrane-distal CEACAM1-L phosphotyrosine motif primarily served to stabilize and sustain the CEACAM1-L/SHP-1 interaction. Finally, our results demonstrate and emphasize the importance of binding kinetics in the action of cellular signalling networks. Some of the fast binding interactions dominated during the first few minutes after CEACAM1-L tyrosine phosphorylation and then disappeared. Since CEACAM1-L tyrosine phosphorylation is transient in some cell types, it is these transient interactions that play a dominant role in initiation of CEACAM1-L-mediated signal cascades. Such fast but transient kinetic interactions most likely have important roles in many other cell signaling events.

6. Acknowledgement

The present investigation was supported by grants from the Swedish Research Council, the Swedish Cancer Foundation, Karolinska Institutet, and the Canadian Institutes of Health Research.

7. References

Beauchemin, N., Kunath, T., Robitaille, J., Chow, B., Turbide, C., Daniels, E., & Veillette, A. (1997). Association of biliary glycoprotein with protein tyrosine phosphatase SHP-1 in malignant colon epithelial cells. *Oncogene,* 14, 783-790.

Brümmer, J., Neumaier, M., Göpfert, C., & Wagener, C. (1995). Association of pp60c-src with biliary glycoprotein (CD66a), an adhesion molecule of the carcinoembryonic antigen family downregulated in colorectal carcinomas. *Oncogene,* 11, 1649-1655.

Gray-Owen, S.D., & Blumberg, R.S. (2006). CEACAM1: contact-dependent control of immunity. *Nature Reviews Immunology,* 6, 433-446.

Huber, M., Izzi, L., Grondin, P., Houde, C., Kunath, T., Veillette, A., & Beauchemin, N. (1999). The carboxyl-terminal region of biliary glycoprotein controls its tyrosine phosphorylation and association with protein-tyrosine phosphatases SHP-1 and SHP-2 in epithelial cells. *J. Biol. Chem.,* 274, 335-344.

Müller, M.M., Klaile, E., Vorontsova, O., Singer, B.B., & Öbrink, B. (2009). Homophilic adhesion and CEACAM1-S regulate dimerization of CEACAM1-L and recruitment of SHP-2 and c-Src. *J. Cell Biol.*, 187, 569-581.

Myszka, D.G., Morton, T.A., Doyle, M.L., & Chaiken, I.M. (1997). Kinetic analysis of a protein antigen-antibody interaction limited by mass transport on an optical biosensor. *Biophys. Chem.,* 64, 127-137.

Öbrink, B., Sawa, H., Scheffrahn, I., Singer, B.B., Sigmundsson, K., Sundberg, U., Heymann, R., Beauchemin, N., Weng, G., Ram, P., & Iyengar, R. (2002). Computational analysis of isoform-specific signal regulation by CEACAM1 - a cell adhesion molecule expressed in PC12 cells. *Ann. N. Y. Acad. Sci.,* 971, 597-607.

Press, W.H., Teukolsky, S.A., Vetterling, W.T., & Flannery, B.P. (1999). *Numerical Recipies in C* (2nd ed), Cambridge University Press, Cambridge, U.K.

Sigmundsson, K., Másson, G., Rice, R., Beauchemin, N., & Öbrink, B. (2002). Determination of active concentrations and association and dissociation rate constants of interacting biomolecules: an analytical solution to the theory for kinetic and mass transport limitations in biosensor technology and its experimental verification. *Biochemistry,* 41, 8263-8276.

Singer, B.B., Scheffrahn, I., Kammerer, R., Suttorp, N., Ergun, S., & Slevogt, H. (2010). Deregulation of the CEACAM expression pattern causes undifferentiated cell growth in human lung adenocarcinoma cells. *PLoS ONE*, 5(1): e8747. doi:10.1371/journal.pone.0008747.

Songyang, Z., Shoelson, S.E., Chaudhuri, M., Gish, G., Pawson, T., Haser, W.G., King, F., Roberts, T., Ratnofsky, S., Lechleider, R.J., Neel, B., Birge, R.B., Fajardo, J.E., Chou, M.M., Hanafusa, H., Schaffhausen, B., & Cantley, L.C. (1993). SH2 domains recognize specific phosphopeptide sequences, *Cell,* 72, 767-778.

Songyang, Z., Shoelson, S.E., McGlade, J., Olivier, P., Pawson, T., Bustelo, X.R., Barbacid, M., Sabe, H., Hanafusa, H., Yi, T., Ren, R., Baltimore, D., Ratnofsky, S., Feldman, R.A., & Cantley, L.C. (1994). Specific motifs recognized by the SH2 domains of Csk, 3BP2, fps/fes, GRB-2, HCP, SHC, Syk, and Vav. *Mol. Cell. Biol.,* 14, 2777-2785.

Waksman, G., Shoelson, S.E., Pant, N., Cowburn, D., & Kuriyan, J. (1993). Binding of a high affinity phosphotyrosyl peptide to the Src SH2 domain: crystal structures of the complexed and peptide-free forms. *Cell,* 72, 779-790.

Weber, T., Schaffhausen, B., Liu, Y., & Günther, U.L. (2000). NMR structure of the N-SH2 of the p85 subunit of phosphoinositide 3-kinase complexed to a doubly phosphorylated peptide reveals a second phosphotyrosine binding site. *Biochemistry,* 39, 15860-15869.

Yang, J., Liu, L., He, D., Song, X., Liang, X., Zhao, Z.J., & Zhou, G.W. (2003) Crystal structure of human protein-tyrosine phosphatase SHP-1, *J. Biol. Chem.,* 278, 6516-6520.

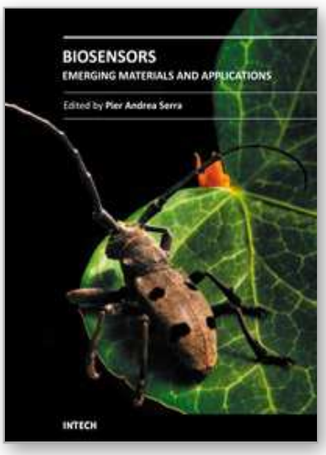

Biosensors - Emerging Materials and Applications
Edited by Prof. Pier Andrea Serra

ISBN 978-953-307-328-6
Hard cover, 630 pages
Publisher InTech
Published online 18, July, 2011
Published in print edition July, 2011

A biosensor is a detecting device that combines a transducer with a biologically sensitive and selective component. Biosensors can measure compounds present in the environment, chemical processes, food and human body at low cost if compared with traditional analytical techniques. This book covers a wide range of aspects and issues related to biosensor technology, bringing together researchers from 19 different countries. The book consists of 27 chapters written by 106 authors and divided in three sections: Biosensors Technology and Materials, Biosensors for Health and Biosensors for Environment and Biosecurity.

INTECH
open science | open minds

InTech Europe
University Campus STeP Ri
Slavka Krautzeka 83/A
51000 Rijeka, Croatia
Phone: +385 (51) 770 447
Fax: +385 (51) 686 166
www.intechopen.com

InTech China
Unit 405, Office Block, Hotel Equatorial Shanghai
No.65, Yan An Road (West), Shanghai, 200040, China
中国上海市延安西路65号上海国际贵都大饭店办公楼405单元
Phone: +86-21-62489820
Fax: +86-21-62489821

IntechOpen